Bidirectional High-Power High-Efficiency non-isolated step-up DC-DC Converter

E. Sanchis-Kilders(1), A. Ferreres(1), E. Maset(1), J.B. Ejea(1), V. Esteve(1), J. Jordán(1), J. Calvente(2), A. Garrigós(3)

(1) Dpt. Ingeniería Electrónica
E.T.S.E. / Universitat de València
Dr. Moliner, 50,
E-46100 Burjassot, SPAIN
e-mail: esteban.sanchis@uv.es

(2) Dpt. d'Enginyeria Electrònica, Elèctrica i Automàtica
E.T.S.E. / Uni. Rovira i Virgili,
E-43007 Tarragona, SPAIN
e-mail: fcalven@etse.urv.es

(3) División Tecnología Electrónica
E.P.S.E. / Uni. Miguel Hernández
Avda. de la Universidad s/n,
E-03202 Elche, SPAIN
e-mail: augarsir@umh.es

Abstract— This paper presents the results of a high-efficiency high-power (5kW) non-isolated bidirectional DC-DC converter. High efficiency, high stability and simplicity are the main goals, and no galvanic isolation is required. The proposed topology is a new BOOST converter with output filter where input and output inductors are coupled together which can be designed to be a minimum phase system. This topology provides therefore input and output current filtering, reducing noise and need of additional filters. Its bidirectionality reduces mass in many applications like in charge/discharge subsystems and lowers cost and component count. This converter is useful with any system that needs backup batteries and therefore has to charge and discharge them properly. It can be applied in space, automotive and telecom application.

I. INTRODUCTION

High power buses used nowadays are normally backed up with batteries, which have to be charged and discharged depending on the bus power demand. These systems are common in telecommunications applications, space platforms and automotive electrical buses. In most part of these applications the power source is a DC voltage and therefore a DC-to-DC converter is needed. Modularity is also required which translates into the ability of connecting modules in parallel easily. Current control solves this requirement and also provides all other typical benefits of current control (inherent short circuit protection, equal current sharing and more stable system). The use of a bidirectional unit saves mass and cost [2], although it adds complexity due to the need to drive a second transistor (in our case, a "floating" drive is needed). In space applications it also requires additional measures to avoid single point failures. Space critical systems (power, attitude, etc) must be single point failure free for unmanned missions and two point failure free for manned missions at the European Space Agency (ESA). A single point failure is defined as a single failure which implies the loss of the system (the power system in our application) [9].

The converter should comply with the following specifications:

Input voltage (battery voltage)	V_{in} = 85V..100V
Output voltage (bus voltage)	V_o = 120V ± 0.5%
(no galvanic isolation required)	
Switching frequency	f_s = 100kHz
Output power	P_o = 5kW
Efficiency	η>95%

Project supported by the Spanish M.C.T. SubD.G.P.I. Ref: ESP 2003-08905

To achieve a high MTBF, two basic principles have to be observed: all components must have a low temperature rise and the circuit must be as simple as possible. One way to assure a high MTBF is to apply strict derating rules [3]

Input and output filtering is becoming more and more stringent and additional filters are needed. This again brings up stability problems. This can be solved by choosing topologies which already integrate these filters.

II. THE COUPLED INDUCTOR BOOST CONVERTER

The selected topology was already introduced in [4], [5] and [6]. This topology is a step up converter, with input inductor and output inductor coupled together. Bidirectionality is achieved by replacing the BOOST diode with a MOSFET and does not affect the control, as long as the control devices are capable of sensing and processing bidirectional currents.

The use of the coupled inductors assures that the converter behaves, from the control point of view, as a minimum phase system and therefore without a right half plane zero, which can create stability problems. These systems can be easily stabilized like the Buck converter. The chosen current control is Conductance Control [1] that can be easily applied by sensing the current flowing through L_b. Parallelizing is then straightforward thank to the current control loop.

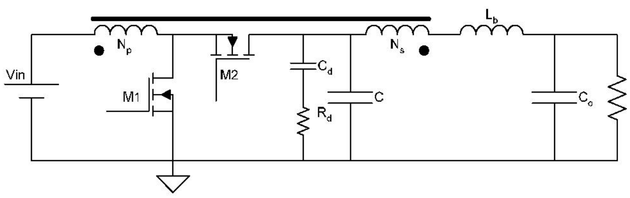

Figure 1. Bidirectional Coupled Inductors' Boost.

Fig. 1 shows the scheme of the converter. It already includes the two MOSFET which permit bidirectional flow of power. As soon as the output voltage increases, due to an additional flow of power to the load from another source (photovoltaic panels or fuel cell, for example; not shown in figure 1), the exceeding power will flow from output to input of the converter and charge the battery (here Vin). If M2 is substituted by a diode pointing to the output like a BOOST diode, the converter would be unidirectional but remain as a non isolated step up converter with minimum phase behavior.

The coupled inductors have been substituted by the model of a transformer with a given magnetizing inductance and leakage inductance. The design of the coupled inductances is explained in [5]. The real components are then a transformer with a designed magnetizing inductance value and an additional output inductance, L_b. Leakage inductance is assimilated to L_b. Energy transfer is done therefore in an inductive and direct way as for example in the buck converter.

Its great advantage compared with the two-inductors-boost converter is that when working as a unidirectional converter its main switch is referred to ground. Energy transfer is done also in an inductive way instead of a capacitive way as in the two-inductor boost [6] what allows more flexibility in terms of the turn ratio of the transformer.

Fig. 2 shows the simulated waveforms of the converter under bidirectional conditions. Output voltage overshoot and undershoot is always below 1%. It can be also noticed that the duty does almost not change (V_{comp} remains constant) because input and output voltage remained the same. Stability is also guaranteed as no undesirable ringing is observed during the transitions. This confirms that the system is a minimum phase system.

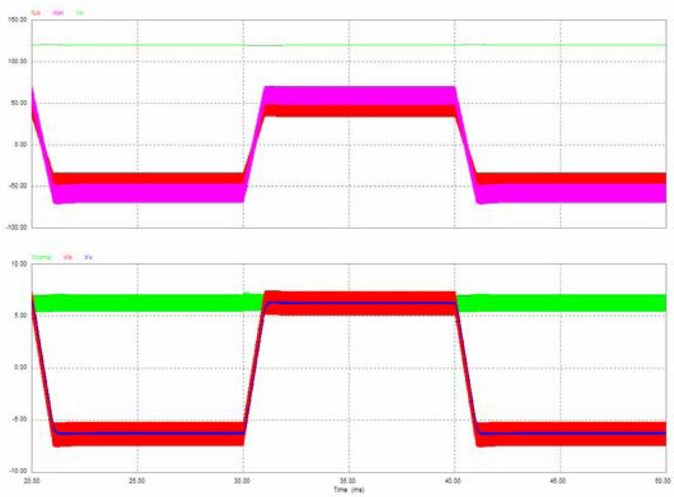

Figure 2. Simulated converter waveforms with changing current direction: a) V_o (green), I_{in} (=Ibat; magenta) and I_{Lb} (=ILo; red) b) V_v (blue), V_{comp} (green) and V_{io} (red), where V_v (blue) is the output of the voltage amplifier, V_{comp} is the output of the current amplifier and signal compared with the triangular waveform and V_{io} is the output of the current sensor.

Fig. 3 shows the simulated waveforms of the converter when power is flowing from the battery to the output. It can be noticed that input and output current are filtered by both inductors. Output voltage is well regulated and the voltage ripple at capacitor C (see Fig. 1) is low as designed (design criterion can be found in [5]). The current through the damping network is also small and therefore the power dissipation in the resistor, R_d, is kept to a minimum (from the design it is only 2.3W which is very small compared to the output power P_o=5kW).

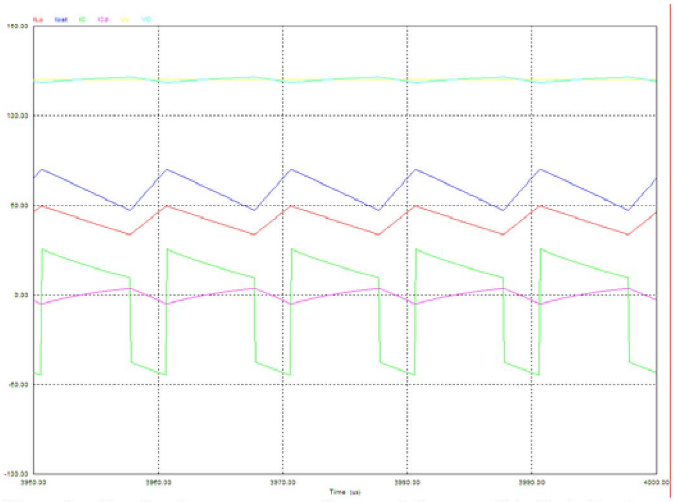

Figure 3. Simulated converter waveforms at full power (P_o): V_o (yellow), I_{in} (=Ibat; blue), I_{Lb} (red), I_C (green), V_C (light blue) and I_{Cd} (magenta). The names are after Fig. 1.

Input and output current is filtered and no additional filters are required with this topology. Due to the fact that the filtering is integrated into the converter no stability problems appear and a Boost-like topology is available without a right half plane zero and additional output filtering.

III. Small Signal Analysis

The coupled inductor BOOST converter has the same DC transfer function as the classical BOOST converter and turns ratio of the magnetic devices does not affect the DC transfer ratio.

$$V_o = \frac{1}{1-D} V_i \tag{1}$$

The damping shown in Fig. 1 is needed for stability purposes and does not theoretically imply appreciable losses (P_{Rd} = 2.5W at P_0 = 5kW). The minimum phase behavior is given only under a certain condition or properly damping the resonance [5]. To not be constrained by this condition (Eq. (2)) we have chosen to add the damping network. This allows us to choose a more convenient turns ratio of the magnetic element.

$$\frac{N_s}{N_p} > \frac{1}{1-D} \tag{2}$$

Classical conductance control has been applied to the converter in order to let it behave as a voltage controlled current source. Feed forward has been also added to compensate for the input voltage variation. The frequency response measured matches very well the calculated bode plots obtained with the classical model.

The small signal analysis leads to a complex expression shown in Eq. (3), but which can be turned to an easy frequency response.

When damping the resonance properly, then the above inequality (Eq. (2)) can be overridden. In fact, damping does not penalize efficiency (only 0.05%) and provides us with smaller inductors by avoiding the fore mentioned condition. By using the design equations given in [5] a perfect and stable behavior can be expected under all load and input voltage range.

Transfer function of the damped circuit, P_d, obtained applying the well-known state-space-averaging method results:

$$P_d(s) = \frac{\tilde{i}_{Lb}}{\tilde{d}} = \frac{V_o}{R_L}\frac{1}{1-D}\frac{A(s)\gamma B(s) + n(1-D)C(s)}{C(s)D(s)+E(s)} \qquad (3)$$

Where the subfunctions used in the previous expression are listed below.

$$A(s) = \left(R_d C_d s + 1\right) \qquad (4)$$

$$B(s) = \left(1-D\right)^2 - \frac{L_{ms}}{n^2 R_L}s \qquad (5)$$

$$C(s) = \left[\left[\frac{L_{ms}}{n^2}C\,s^2 + \left(1-D\right)^2\right]A(s) + \frac{L_{ms}}{n^2}C_d s^2\right] \qquad (6)$$

$$D(s) = L_{ds}C_o s^2 + \frac{L_{ds}}{R_L}s + 1 \qquad (7)$$

$$E(s) = \gamma^2 \frac{L_{ms}}{n^2 R_L} s\left(R_L C_o s + 1\right)A(s) \qquad (8)$$

The variables used agree with the circuit depicted in Fig. 1. R_d and C_d for the damp circuit, L_{ms} is the magnetizing inductance of the transformer reflected to secondary, L_{ds} is the leakage inductance of the secondary (very small) which has to be increased with an additional inductor (very large and therefore L_{ds}=L_b), the turns ratio of the transformer $n=N_s/N_p$, and a coefficient $\gamma=1-n(1-D)$.

IV. Circuit Design

A prototype (P_o=5kW) has been built to check the real circuit. High quality components have been used and discrete control has been built to have a higher flexibility. A four layer PCB with additional copper deposition (to cope with the high circulating currents) has been designed and high power density has been achieved.

The simplified circuit of the unit is shown. Soft switching circuit has been studied but no good results have been reached and therefore its use has been discarded [11]. To drive both MOSFET the same isolated driving circuit has been used to assure symmetrical behavior.

Fig. 4 shows the power circuit of the prototype with the real values used. Body diodes of the MOSFET are not shown although present in the real circuit. Q1 is driven with a PWM signal that has a duty cycle D and Q2 with the complementary signal.

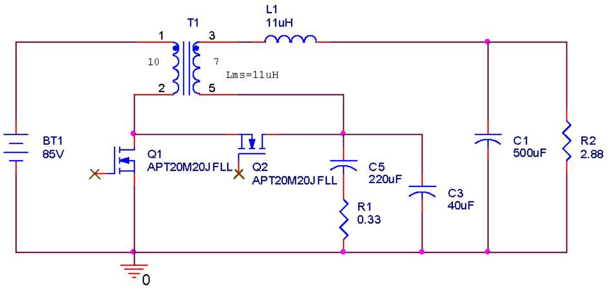

Figure 4. Circuit diagram of the 5kW prototype. The turns ratio of the transformer is 10:7 and the magnetizing inductance seen from the secondary (N_s=7) was designed as L_{ms}=11μH

The control circuit is shown in Fig. 5 where two control loops are implemented. Current is measured by the commercial sensor LEM LA100-P/SP13 and the whole circuit is implemented with discrete devices to take advantage of a greater flexibility. We have also to keep in mind that in space applications only space qualified parts may be used. Almost all components used in our design have its space qualified counterpart. The FET Pulse drive used to drive the MOSFET on a floating way is described more in detail in [8].

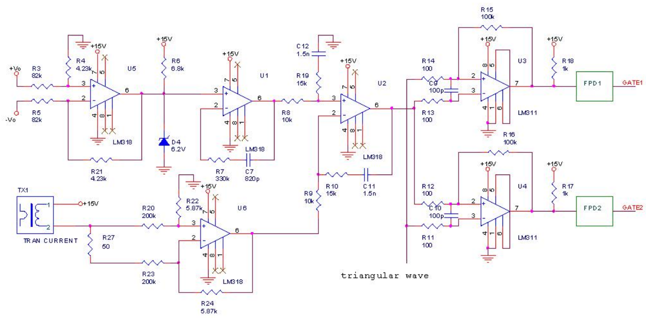

Figure 5. Feedback loop circuit. The block FPD is a FET Pulse Drive circuit which is able to generate bipolar isolated signals ranging from 0% to 100% duty cycle. One of them is not necessary but has been added to equalize delays.

The triangular wave generator has been designed based on current mirrors used as current sources. Current diodes could also have been used but are more expensive and more difficult to find. This circuit (Fig. 6) is able to generate precise waveforms for frequencies above 200kHz. Feed forward which only increases the upper peak of the waveform is achieved by injecting input voltage into the first current mirror.

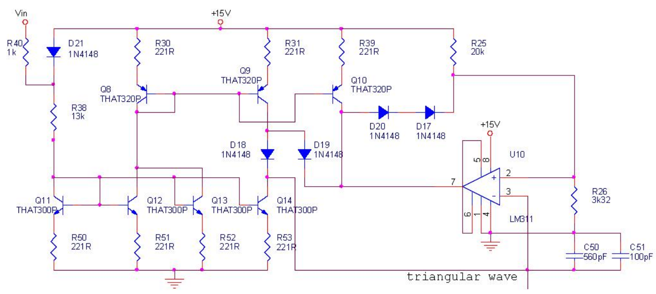

Figure 6. Triangular wave generator based on current mirrors which is able to generate signals above 200kHz without distortion.

Difference amplifiers have been added to all sensed signals to increase signal-to-noise ratio. This practice is highly recommended at higher power levels.

V. EXPERIMENTAL RESULTS

The experimental results obtained are presented in this section. It will be demonstrated that the prototype built has a very nice behavior and has achieved a very high efficiency.

The experimental results have shown that losses in the damping resistor R_d were much larger than expected mainly due to large switching noise which increased the rms voltage across it. Anyhow this did not affect the efficiency but only the selection of this resistor. As can be seen in the circuit a much larger set of parallel connected resistors were needed to dissipate the power (we estimated that it was around 6W).

A. Frequency response

First we will present the frequency responses, not only for the current loop but also for the overall loop (current loop closed and voltage loop open).

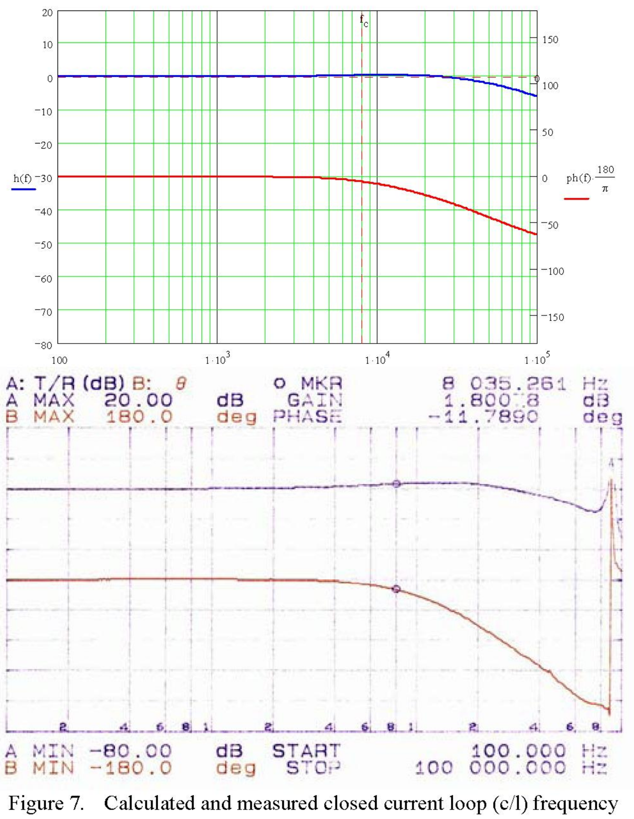

Figure 7. Calculated and measured closed current loop (c/l) frequency response of the converter with at P_0 = 4kW and V_{in}=85V. It is clearly seen that the model matches very good the built unit. The current loop behaves as a current source at least up to 8kHz with little phase degradation.

It is clearly seen in Fig. 7 that the system looks like a current source. Its has a flat behavior with a very small phase degradation up to the crossover frequency of the whole system, that as we will see reaches up to 8kHz.

The overall frequency response is shown in Fig. 8 where we again see that it looks like a first order system. Cross over frequency is higher in the real prototype than the one obtained and designed out of the model. Although only one frequency response has been presented the measurement has been repeated for different power levels and different input voltages. The result has been very good and phase margin and cross over has only a small variation (phase margin goes from 87° to 74° and bandwidth from 7.6kHz to 8.5kHz). The system is stable over all the output power and input voltage range.

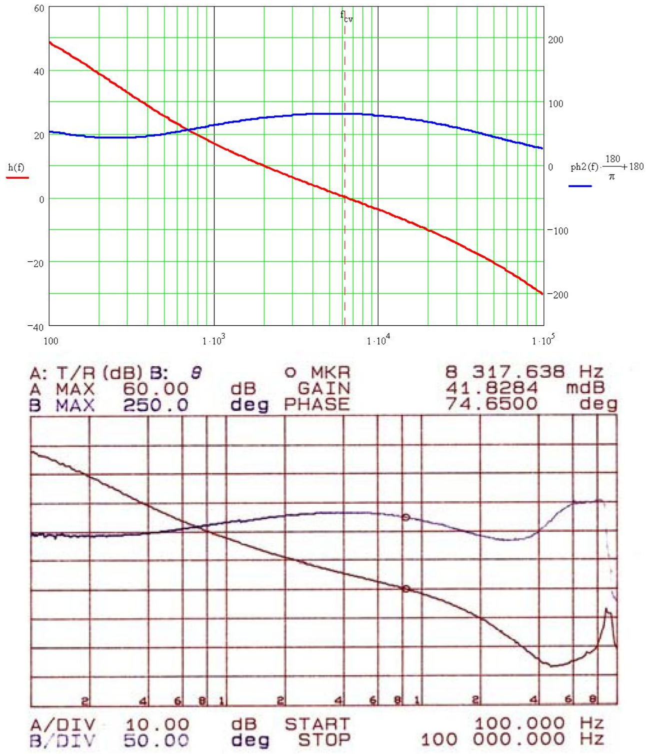

Figure 8. Calculated and measured open loop (o/l) frequency response of the whole converter at P_0 = 5kW and V_{in}=85V. Experimental bandwidth reaches 8.3kHz and phase margin is more than 74°, although the design was made for 6.3kHz and a phase margin of 82°.

Bandwidth reached is f_{BW}=8.3kHz and phase margin is 74°.

Output impedance has also been measured to see if the required levels of ESA are fulfilled [9]. This requirement defines a mask which assures that under a 50% output current modulation the voltage overshoot is smaller than 1%. Using a special setup which uses a power MOSFET which is used in its active region we have modulated the output current of the converter and measure the output voltage. The measured frequency response is within the limits established by the ESA mask. Fig. 9 shows the calculated impedance curve and the measured curve. The mask has been also added.

The measured curve shows a small heap at about 12kHz whose origin we are investigating. Although this small heap does not appear in the model which does not take into account this parasitic effect in the experimental diagram we see that it is still within the mask and it does not affect the behavior of the converter or its stability.

The maximum output impedance is 46mΩ. This assures that under a 50% load change the output voltage overshoot is always below 1%.

$$\Delta V_0 = \sqrt{\frac{P_0 Z_{0\max}}{200}} = \sqrt{\frac{5kW\ 46m\Omega}{200}} = 1.07V \qquad (9)$$

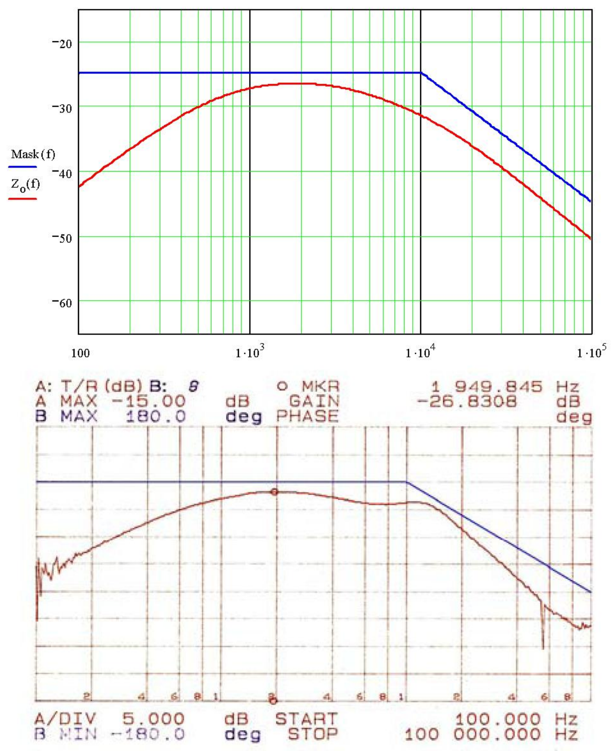

Figure 9. Calculated and measured output impedance of the converter at P_0 = 2kW and V_{in}=100V. The maximum is at 1.9kHz and reaches 46mΩ satying always within the required mask. Experimentally we see that a small heap appears at about 12kHz which is due to parasitic effects of the converter.

To assure that the impedance is correctly measured we have also made a load step of 3kW (from 2kW up to 5kW) and have measured the output voltage ripple. This has to confirm the results shown by the impedance curve.

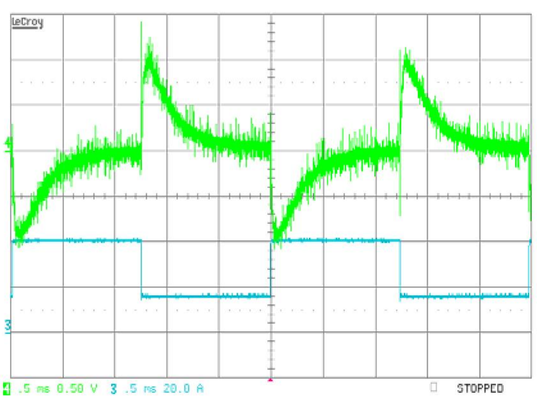

Figure 10. Measured output voltage ripple when applying an output current step of 24A (at 400Hz) and at V_{in}=85V. Ch3: I_0 (20A/div), Ch4: ΔV_0 (0.5V/div).

Load step confirms the good first order behavior of the converter. Please note that the load step used at this stage is slightly larger than 50% and reaches 58%.

B. Waveforms

MOSFET were switched in a hard way obtaining good results. Although some ringing appears in the waveforms this does not degrade the overall behavior of the converter. Increase of noise or instabilities were not observed at this time. No snubber circuits were put in place to reduce the ringing at this stage. Passive snubber circuits would surely reduce ringing and show nicer waveforms but for sure result in reduction of efficiency.

Switching waveforms at both MOSFET are shown in Fig. 11. Worst case conditions have been selected (V_{in}=85V and P_0=5kW).

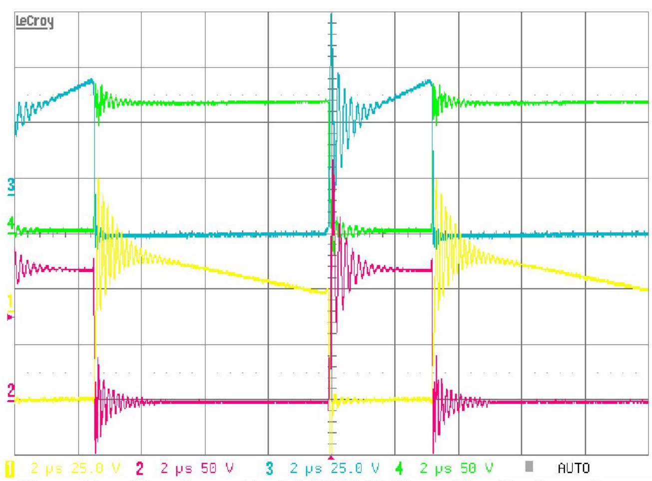

Figure 11. Waveforms at both MOSFET. V_{DS} and I_D of both are shown here. Ringing during commutation is seen. Measured at V_{in}=85V and P_0=5kW. Ch1: I_{D2} (25A/div), Ch2: V_{DS2} (50V/div), Ch3: I_{D1} (25A/div), Ch4: V_{DS1} (50V/div).

To see how much switching losses we can expect in our switches we have measured the safe operating area (SOA) of both devices under worst case conditions, that is at V_{in}=85V and P_0=5kW.

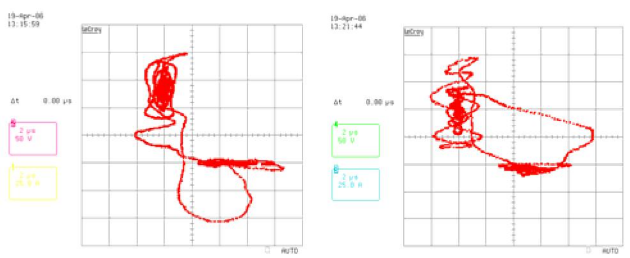

Figure 12. SOA of both MOSFET measured at V_{in}=85V and P_0=5kW. Left: SOA of Q2 where Ch1: I_{D2} (25A/div), Ch2: V_{DS2} (50V/div). Right: SOA of Q1, Ch3: I_{D1} (25A/div), Ch4: V_{DS1} (50V/div).

SOA of both transistors shows that the transistor which shows more ringing as seen in Fig. 11 (Q1) seems to have a much softer switching than Q2, which has much less ringing. Anyhow losses have proved to be very low in both transistors as seen in the efficiency curves.

Output ripple of the converter has also been measured and is shown in Fig. 13.

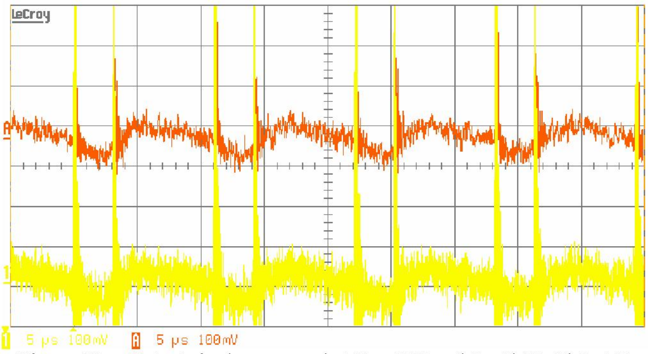

Figure 13. Output ripple measured at V_{in}=85V and P_0=5kW. Ch1: ΔV_0 (100mV/div) ad ChA: Ch1 filtered and with same scale.

Output ripple at maximum power and minimum voltage is about 100mV which is less than 0.1%. If noise is taken into account spikes reach about 2V peak-to-peak although noise measurements have always to be done with special care.

C. *Efficiency*

Efficiency has been measured in direct operation and no differences are expected to occur under inverse operation. The presented efficiency figures have been obtained including the losses of the control although the losses of an auxiliary power supply needed to generate this control voltage have not been considered. In any case specifications have been met and efficiency is always higher than 97%.

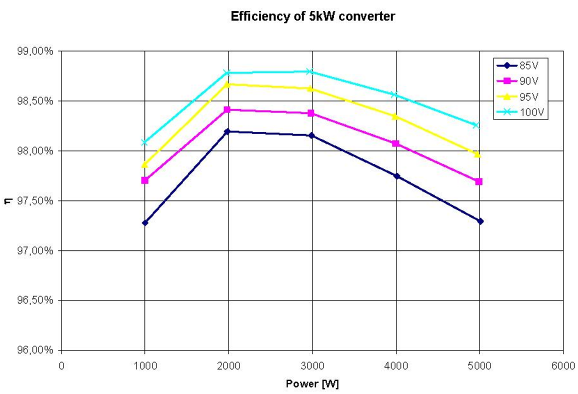

Figure 14. Efficiency of the 5kW hard switching prototype.

If fine tuning switching behavior of both transistors probably some additional losses could be saved and efficiency could be increased at the high power end of the curves. Also one driving circuit could be replaced by a simple push-pull bipolar transistors driver configuration, which saves one of the isolated driver used now for symmetry purposes (and its losses).

D. *Bidirectional operation*

The test setup for the bidirectional converter is shown in Fig. 15. We have used two power supplies that must be capable of delivering at least the full power of the converter plus the first load step. In case the converter has a 5kW power rating and the load steps are of 1kW, the power supplies must deliver 6kW. At least one of the power supplies must be able to work in current mode. This setup allows us to test the bidirectional behavior of the converter. The input power source would be "V_{in}" together with "R_{Lin}" and works in voltage source mode. "R_{Lin}" is the current sinking device when in reverse mode in case that the input power supply is not capable of sinking current (which is normally the case). The output represents the bus where its voltage is V_0 and its load $R_{L\ bus}$. If the bus is fed by another energy source ($I_{extra\ bus}$) then the Device Under Test (DUT=our converter) must deliver less power to the load R_{Lbus}. If we increase $I_{extra\ bus}$ up to 6kW and $R_{L\ bus}$ consumes 1kW of power, then the DUT keeps the bus voltage regulated at V_0 and the converter is having 5kW of power flowing in reverse direction (into the battery V_{in}). As explained, R_{Lin} will drain current flowing from the output to the input. But V_{in} must be kept connected to regulate the input voltage (the converter regulates the output voltage, V_0, and behaves as an current source at the input).

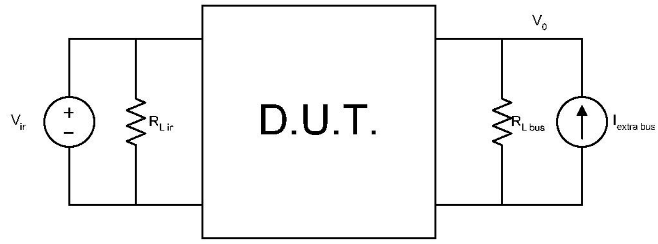

Figure 15. Test setup for the bidirectional converter (Device Under Test).

In Fig. 16 we see the waveforms of the converter in reverse operation. The current through both MOSFET is negative. Due to the values we had available for R_{Lin} we could only test the converter up to 2.5kW of reverse power.

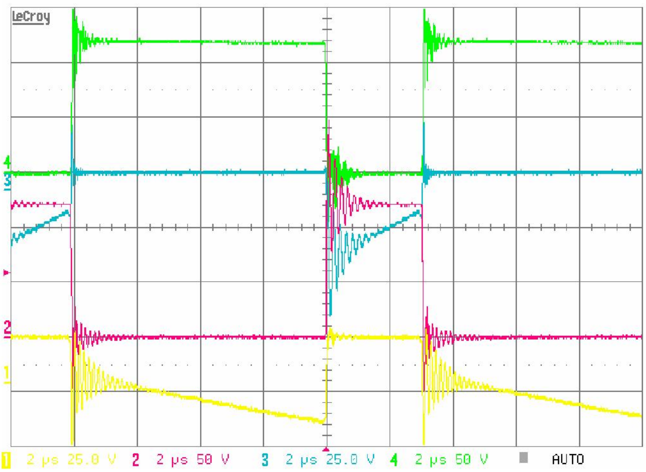

Figure 16. Waveforms of the MOSFET in reverse operation (P_0=-2.5kW; Ch1: I_{D2} (25A/div), Ch2: V_{DS2} (50V/div), Ch3: I_{D1} (25A/div), Ch4: V_{DS1} (50V/div)) operation. Ringing appears as in direct operation. V_{in}=85V.

It can be clearly seen in Fig. 16 that ringing is the same as when working in direct operation.

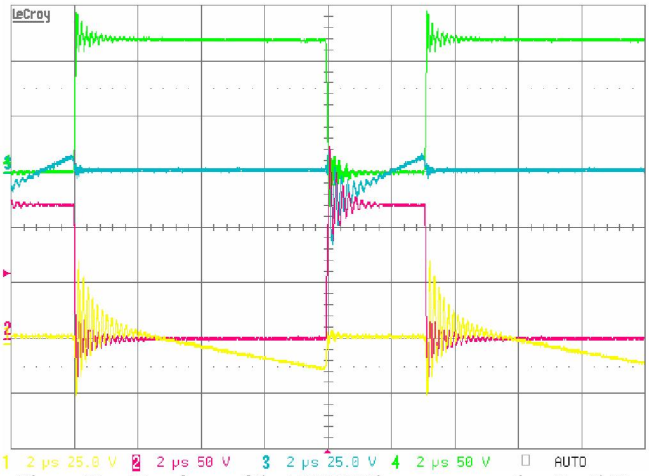

Figure 17. Waveforms of the MOSFET in reverse operation (P_0=0kW; Ch1: I_{D2} (25A/div), Ch2: V_{DS2} (50V/div), Ch3: I_{D1} (25A/div), Ch4: V_{DS1} (50V/div)) operation. Ringing appears as in direct operation. V_{in}=85V.

Fig. 17 shows the waveforms in the MOSFET when the input power equals the output power. Only ripple current is present and average values of current are equal zero.

All operating points of the converter in direct or reverse operations were completely stable and output voltage was always regulated.

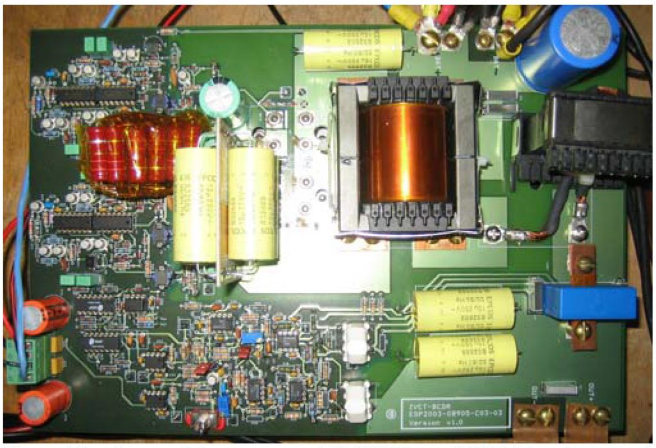

Figure 18. Image of the prototype. MOSFET have SOT-227 packages and are underneath the PCB.

VI. Conclusion

A new topology is being proposed and tested at 5kW to provide optimum results as bidirectional step up DC-DC converter. The converter is a coupled inductor BOOST with output filter. When coupling its two inductors and damping the resonance, a minimum phase system results. Stability of the converter has been measured and the model has proved to be very accurate. Bidirectionality has successfully been demonstrated and an efficiency of always more than 97% has been achieved. At system level this topology saves volume, mass and cost not only due to its Bidirectionality but also because no additional input or output filtering is needed.

Acknowledgment

The authors would like to thank:

- Spanish Ministry of Science and Technology (SubD.G.P.I.) which has supported this research with the project ref: ESP 2003-08905-C03-03.
- Regional Government of Valencia (Conselleria d'E. U. i C.) which has supported this research with the projects ref: ACOMP06/025 and GRUPOS05/076
- LEM and Mr. Stefan Lüscher for providing us with samples for the prototype and good advices for the right selection of the current transducer.
- THAT Corporation for providing us with samples of matched bipolar transistors.

References

[1] D. O'Sullivan, H. Spruyt, A. Crausaz, "PWM Conductance Control", *IEEE PESC Conf. 1988*, pp. 351-359, 1988.
[2] S. H. Weinberg, A. López, "A Bidirectional BDR/BCR for Satellite Applications", *5th European Space Power Conference 1998*, ESA SP-416, pp.27-32, September 1998.
[3] "Derating and end-of-life parameter drifts. Electrical, electronic and electromechanical components", *ESA ECSS-Q-60-11*, http://www.ecss.nl
[4] J. Calvente, L. Martinez-Salamero, P. Garces, R. Leyva, A. Capel; "Dynamic optimization of bidirectional topologies for battery charge/discharge in satellites"; *IEEE PESC Conf., 2001*. Vol.4, pp.1994-1999.
[5] J. Calvente, L. Martinez-Salamero, H. Valderrama, E. Vidal-Idiarte, "Using Magnetic Coupling to Eliminate Right Half-Plane Zeros in Boost Converters", *IEEE Power Electronics Letters*, Vol. 2 (Nº2), pp.58-62, June 2004
[6] P. Rueda, S. Ghani, P. Perol, "A New Energy Transfer Principle to achieve a Minimum Phase & Continuous Current Boost Converter", *IEEE PESC Conf., 2004,* pp.2232-2236.
[7] E. Sanchis-Kilders, A. Ferreres, E. Maset, J.B. Ejea, V. Esteve, J. Jordán, R. García, A. Garrigós, "High Power Passive Soft Switched Interleaved Boost Converters", *IEEE PESC Conf., 2004,* pp.426-432.
[8] A.Crausaz, E.Gasquet, E.Sanchis. "Power MosFet: ESA Driving Licence", 4th *European Space Power Conference 1995*, ESA SP-369, pp.227-233, September 1995.
[9] "Power Standard", *ESA PSS-02-10*, http://www.esa.int/SPECIALS/ESA_Publications/index.html
[10] E. Sanchis-Kilders, J.B. Ejea, A. Ferreres, E. Maset, V. Esteve, J. Jordán, J. Calvente, A. Garrigós, "Bidirectional Coupled Inductors Step-up Converter for Battery Discharging-Charging", *IEEE PESC Conf., 2005,* pp.64-68.
[11] E. Sanchis-Kilders, A. Ferreres, E. Maset, J.B. Ejea, V. Esteve, J. Jordán, A. Garrigós, J. Calvente, "Soft Switching Bidirectional Converter for Battery Discharging-Charging", *IEEE APEC Conf., 2006,* pp.603-609.